Resonance Raman Study of Short-Time Photodissociation Dynamics of the Charge-Transfer Band Absorption of Nitrobenzene in Cyclohexane Solution

Xin-Ming Zhu[†], Shu-Qiang Zhang[†], Xuming Zheng,*[,†] and David Lee Phillips*[,‡]

Department of Applied Chemistry, Zhejiang University of Sciences, Second Road, Xia Sha Gao Jiao Yuan Qu Hangzhou 310033, People's Republic of China, and Department of Chemistry, The University of Hong Kong, Pokfulam Road, Hong Kong S.A.R., People's Republic of China

Received: December 8, 2004; In Final Form: February 5, 2005

Resonance Raman spectra were obtained for nitrobenzene in cyclohexane solution with excitation wavelengths in resonance with the charge-transfer (CT) band absorption spectrum. These spectra indicate that the Franck−Condon region photodissociation dynamics have multidimensional character with motion mainly along the nominal NO_2 symmetric stretch mode (ν_{11}), the nominal benzene ring stretch mode (ν_7), accompanied by a moderate degree of motion along the nominal ONO symmetry bend/benzene ring stretch mode (ν_{23}), the nominal C−N stretch/benzene ring breathing mode (ν_{16}), the nominal CCC bending mode (ν_{20}) and the nominal CCH in-plane bending mode (ν_{14}). A preliminary resonance Raman intensity analysis was done and the results for nitrobenzene were compared to previously reported results for several nitroalkanes.

Introduction

Nitroalkanes and nitroaromatic compounds are of interest as energetic molecules that can have applications as explosive materials[1,2] and may have a possible role in atmospheric chemistry.[3,4] This has led to extensive experimental and theoretical studies of the dissociation and photodissociation of nitroalkanes and nitroaromatics.[5−28] Nitroalkanes have absorption bands near ∼200 nm (called the B-band absorption) that have been assigned to an allowed $X(^1A_1) \rightarrow {}^1B_2$ or $\pi \rightarrow \pi^*$ transition that is localized on the NO_2 group on the basis of several experimental and theoretical investigations.[5−10] Excitation of the nitroalkanes within the B-band absorption leads mostly to cleavage of the C−N bond with an almost unity quantum yield, even though the NO_2 group is initially excited and typically produces NO_2 (major channel) and NO (minor channel) fragments.[11−14] The broad and structureless B-band absorption observed for both gas- and solution-phase nitromethane and other nitroalkanes suggests that the total electronic dephasing is mostly due to photodissociation before the first vibrational recurrence takes place. The observation of NO fragments in the minor product channel involves a secondary dissociation of the NO_2 and/or the isomerization of nitromethane to methyl nitrite, CH_3ONO, prior to dissociation.[14,15] Resonance Raman spectroscopy has been used to investigate the short-time photodissociation dynamics of nitroalkanes in the gas, liquid, and glass phases within the B-band absorption.[13,16−19] The B-band resonance Raman spectra of nitromethane were similar to each other in the gas, liquid, and glass phases and exhibited a large overtone progression in the nominal NO_2 symmetric stretch mode and relatively weak combination band progressions of the C−N stretch fundamental, the ONO symmetric bend fundamental and two quanta of the NO_2 antisymmetric stretch mode with the overtones of the NO_2 symmetric stretch mode.[13,16,17] Larger nitroalkanes have been examined in the gas and liquid phases and their Franck−Condon region photodissociation dynamics were found to be similar to that of nitromethane.[18,19]

Nitrobenzene has a transition-allowed absorption band near ∼250 nm (called the CT band absorption) that has been assigned to a $1\ {}^1A_1 \rightarrow 2\ {}^1A_1$ or π(benzene ring) $\rightarrow \pi^*(NO_2)$ transition on the basis of experimental and theoretical investigations.[20,21] A gas-phase photolysis study of nitrobenzene with excitation wavelengths between 220 and 280 nm found three primary dissociation pathways.[22] Two of the pathways were $C_6H_5NO_2 \rightarrow C_6H_5 + NO_2$ and $C_6H_5NO_2 \rightarrow C_6H_5NO + O$ and the third pathway involved NO production. It was proposed that the nitrobenzene molecule first isomerized to phenyl nitrite, C_6H_5-ONO, and subsequently decomposed by breaking the C−ONO bond to release NO_2, or the O−NO bond to produce NO, or the ON−O bond to form O.[22] Ab initio calculations were performed and provided further support for the rearrangement pathway as the most likely dissociation channel for the production of NO.[23] The barrier height for the rearrangement of nitrobenzene to phenylnitrite was determined through the characterization of the transition state.[24] The NO_2 and NO loss channels have also been observed for three nitrotoluene isomers.[25−28] Significant OH production was observed in the dissociation of *o*-nitrotoluene and was attributed to an "ortho effect" that involves a bicyclic intermediate and subsequent rearrangement to the nitrite form prior to fragmentation.[27] The product internal energy distributions in the NO fragment from dissociation of *o*-nitrotoluene between 224 and 238 nm were noted to be different from those of the NO fragments produced from dissociation of nitrobenzene or NO_2.[28]

In this paper, we investigate the Franck−Condon region photodissociation dynamics of nitrobenzene in cyclohexane solution by using resonance Raman spectroscopy. The CT-band absorption of nitrobenzene is different from the B-band absorption of nitromethane in that it leads to an internal charge transfer from the benzene ring to the NO_2 group while the B-band absorption of nitromethane is localized on the NO_2 group. This

* To whom correspondence should be addressed: (D.L.P.) telephone 852-2859-2160, fax 852-2857-1586, e-mail phillips@hkucc.hku.hk; (X.Z.) fax 86-0571-86843000, e-mail xzheng@mail.hz.zj.cn.
† Zhejiang University of Sciences.
‡ The University of Hong Kong.

10.1021/jp0444114 CCC: $30.25
Published on Web 03/15/2005

allows a comparison of how the different type of substitution would affect the Franck−Condon region photodissociation dynamics and energy partitioning among the internal degrees of freedom for these different types of nitro compounds in the Franck−Condon region.

Experimental and Computational Methods

Fourier Transform Infrared, Fourier Transform Raman, and Resonance Raman Experiments. The FT-IR spectrum of nitrobenzene in neat liquid was acquired with 2 cm^{-1} resolution (Perkin-Elmer 1 FT-IR spectrometer). The FT-Raman spectrum of neat liquid nitrobenzene was obtained with 2 cm^{-1} resolution and 532 nm excitation (Thermo Nicolet FT-Raman 960 Spectrometer).

To avoid the aggregation of nitrobenzene in cyclohexane solution, a concentration-dependent UV/vis experiment was carried out. The UV/vis spectra showed no discernible changes from about 0.002 to 0.030 M but some changes appeared above 0.050 M, possibly due to aggregation. The resonance Raman experiments used concentrations in the 0.007−0.015 M range for nitrobenzene in cyclohexane solvent so as to avoid possible appreciable aggregation. The power dependence of the resonance Raman spectra was tested and a lower power was used during the resonance Raman measurements to avoid saturation effects and other problems associated with high peak powers. Depletion of the ground-state species could lead the Raman band intensities of the sample relative to those of the solvent to change as the laser power increases. High peak power can also produce more photochemical intermediates or cause the two-photon ionization processes to occur during the laser pulse. These may possibly interfere with the absolute Raman cross section measurements.[29]

The methods and experimental apparatus used for the resonance Raman experiments have been described elsewhere[30−43] so only a short description will be given here. The harmonics of a nanosecond Nd:YAG laser and their hydrogen Raman-shifted laser lines produced the excitation wavelengths used in the resonance Raman experiments. The excitation laser beam was loosely focused to about a 0.5 mm diameter spot size onto a flowing liquid stream of sample. A backscattering geometry was used for sample excitation and for collection of the Raman scattered light by reflective optics. The Raman scattered light was imaged through a polarizer and entrance slit of a 0.5 m spectrograph whose grating dispersed the light onto a liquid nitrogen-cooled charge-coupled device (CCD) mounted on the exit of the spectrograph. The CCD acquired the Raman signal for about 90−120 s before being read out to an interfaced PC computer. About 10−30 of these scans were summed to obtain the resonance Raman spectrum. The Raman shifts of the resonance Raman spectra were calibrated by use of the known vibrational frequencies of the cyclohexane solvent Raman bands. The solvent Raman bands were subtracted from the resonance Raman spectra by use of an appropriately scaled solvent spectrum. Spectra of an intensity-calibrated deuterium lamp were used to correct the resonance Raman spectral intensities for the variation in detection efficiency as a function of wavelength. Portions of the resonance Raman spectra were fit to a baseline plus a sum of Gaussian bands to obtain the integrated areas of the Raman bands.

The absolute Raman cross sections of the nitrobenzene resonance Raman spectra were determined relative to the 802 cm^{-1} Raman band of the cyclohexane solvent. An ultraviolet/visible (UV/vis) spectrometer was used to determine the concentrations of the nitrobenzene sample before and after each measurement and the absorption spectra changed by <5% due to photodecomposition and/or solvent evaporation. The absolute Raman cross sections were computed from the average concentration before and after three measurements by finding the mean of three trials to get a final value for the excitation wavelengths determined.

Time-Dependent Wave Packet Calculations To Model the Resonance Raman Intensities and Absorption Spectrum and Density Functional Theory Calculations. The absorption spectrum and resonance Raman intensities were modeled by use of Heller's time-dependent wave packet approach to resonance Raman scattering.[44−47] The absorption spectrum was calculated from

$$\theta_A(E_L) = (4\pi e E_L M_0^2/3n\hbar c)\int_{-\infty}^{\infty} G(\delta)\, d\delta\, Re \int_0^{\infty} dt\, \langle 0|0(t)\rangle \times \exp[i(E_L + \epsilon_0)]t/\hbar \times \exp[-\Gamma t/\hbar]$$

The resonance Raman intensities are calculated from

$$\sigma_A(E_L) = (8\pi e^4 E_S^3 E_L M_0^4/9\hbar^6 c^4)\int_{-\infty}^{\infty} G(\delta)\, d\delta \times \left|\int_0^{\infty} dt\, \langle f|0(t)\rangle \exp[i(E_L + \epsilon_0)]t/\hbar \times \exp[-\Gamma t/\hbar]\right|^2$$

where E_L is the incident photon energy, M_0 is the transition length evaluated at the equilibrium geometry, f is the final state for the Raman scattering, and n is the solvent index of refraction. The term $\exp[-\Gamma t/\hbar]$ is a homogeneous damping function that has contributions from the excited-state population decay and pure dephasing. $G(\delta)$ is an inhomogeneous distribution of transition energies. $|0(t)\rangle = e^{-iHt/\hbar}|0\rangle$, which is $|0\rangle$ propagated on the excited-state surface for a time t, and H is the excited-state vibrational Hamiltonian.

The ground- and excited-state potential energy surfaces were simulated by harmonic oscillators with their minima set apart by an amount Δ (with dimensionless units for the ground-state normal coordinates). The simple model used in the present study did not employ Duschinsky rotation[46,47] of the normal modes, and the ground- and excited-state harmonic oscillators had the same vibrational frequency. The resonance Raman intensities of the first several overtones as well as the combination bands and the absorption spectrum are determined mainly by the slope of the excited-state surface in the Franck−Condon region in the absence of any vibrational recurrences. The featureless gas- and solution-phase A-band absorption spectra of nitrobenzene suggest that the total electronic dephasing and/or population decay takes place prior to the first vibrational recurrence of any Franck−Condon active modes. For the resonance Raman bands observed in our experimental spectra, the $\langle f|I(t)\rangle$ overlaps decay and has a negligible value after 30 fs. The effects of solvent dephasing used a simple exponential decay term, ($\exp[-t/\tau]$). The bound harmonic oscillator model employed here only provides a convenient method to simulate the Franck−Condon region portion of the excited-state surface that determines the resonance Raman intensities and absorption spectrum and does not in any way imply that the excited state is bound.

Density functional theory (DFT) calculations[48,49] were done to find the optimized geometry and vibrational frequencies as well as the electronic transition energies for the ground or excited electronic states of nitrobenzene. Complete geometry optimization and vibrational frequency computations were computed at the B3LYP/cc-PVTZ level of theory with a C_{2v} symmetry, while the electronic transition energies were calculated at B3LYP-TD/cc-PVTZ. All of the density functional theory calculations made use of the Gaussian program suite.[50]

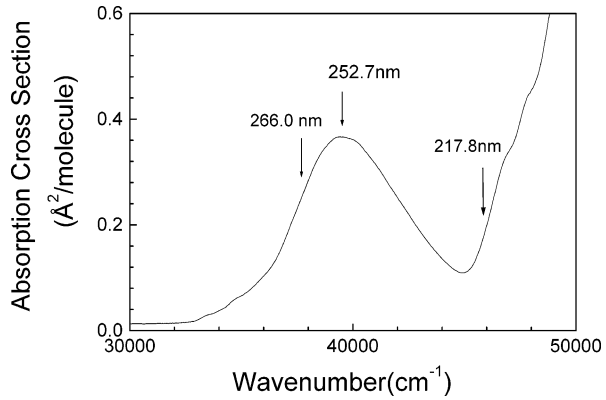

Figure 1. Absorption spectrum of nitrobenzene in cyclohexane solution. The excitation wavelengths used for the resonance Raman experiments are indicated above the absorption spectrum.

TABLE 1: B3LYP-TD/cc-PVTZ-Computed Singlet Transition Energies of Nitrobenzene

		ΔE/eV		f	
state (C_{2V})	character	calcd	exptl	calcd	exptl
1 $^1A_2$	$^1(n,\pi^*)$	3.85 (322 nm)	3.65	0.0000	0.003
1 $^1B_1$	$^1(n,\pi^*)$	4.34 (286 nm)		0.0001	
1 $^1B_2$	$^1(\pi,\pi^*)$	4.46 (278 nm)	4.38	0.0139	0.01
2 $^1A_1$	**^{1}CT or $^1(\pi,\pi^*)$**	**4.86 (255 nm)**	**5.17**	**0.1962**	**0.17**
2 $^1B_2$	$^1(\pi,\pi^*)$	6.00 (207 nm)		0.0001	
3 $^1B_2$		6.12 (203 nm)	6.42	0.0584	0.38

Results and Discussion

UV Spectrum and Electronic Structures of Nitrobenzene. Figure 1 shows the absorption spectrum of nitrobenzene in cyclohexane solution with the excitation wavelengths for the resonance Raman experiments indicated above the absorption spectrum. The spectrum is broad and featureless in both the gas and solution phases.[22] Table 1 lists the B3LYP-TD/cc-PVTZ-computed electronic transition energies and their oscillator strengths for nitrobenzene. The results show an electronically transition-allowed band at 255 nm with an oscillator strength $f = 0.1962$. This is in good agreement with the experimentally measured molar extinction coefficient of $\epsilon \sim 7000$ L/mol·cm or $f = 0.17$ for nitrobenzene. The band at 252 nm was assigned to a charge-transfer excitation between the benzene ring and the nitro group on the basis of our present B3LYP-TD/cc-PVTZ computations and the electron-energy-loss spectroscopy and previously reported CASPT2 computational results.[21] Similarly, the small bands near 280 nm region were assigned to a $^1(n,\pi^*)$ state. Our 252.7 and 266 nm excitation wavelengths used in the resonance Raman experiments should mostly be on resonance with the CT band, while 217.8 nm excitation is mainly on resonance with the high-lying excited state.

CT-Band Resonance Raman Spectra of Nitrobenzene. The vibrational spectroscopy of nitrobenzene has been the subject of numerous studies. Overall assignments of the fundamental frequencies of nitrobenzene were made first by Green and co-workers[51] and Stephenson and co-workers.[52] Later, Green and Harrison[53] revised the assignment of some fundamentals based on polarization and isotope experiments. Recently Clarkson and Smith[54] carried out a DFT analysis of the vibrational spectra of nitrobenzene in order to account for a clear assignment of the nitro bands and to give new insights into the coupling of the nitro and benzene modes. We measured the FT-IR and FT-Raman spectra of neat nitrobenzene and they are shown in Figure 2. Table 2 presents the experimental and B3LYP/cc-PVTZ-computed vibrational frequencies. The notations and assignments of vibrations were made to nitrobenzene according to the work of Clarkson and Smith.[54] Our experimental spectra and DFT computational results are in good agreement with previous work on the vibrational spectroscopy of nitrobenzene[51−54] and in particular with that of Clarkson and Smith.[54] Figure 3 shows an overview of the CT-band resonance Raman spectra of nitrobenzene obtained with 266.0, 252.7, and 217.8 nm excitation wavelengths. While the 266 and 252.7 nm resonance Raman spectra are similar to each other, the 217.8 nm resonance Raman spectrum displays a very different intensity pattern than the 252.7 and 266 nm spectra. It is interesting to note that the most intense vibrational mode in the 217.8 nm resonance Raman spectrum is 1002 cm^{-1}. We expect that the preresonance interference to the CT band from a higher-lying state is not very strong since the 217.8 nm resonance intensity pattern is very different from the 252.7 and 266 nm spectra, which are very similar to one another.

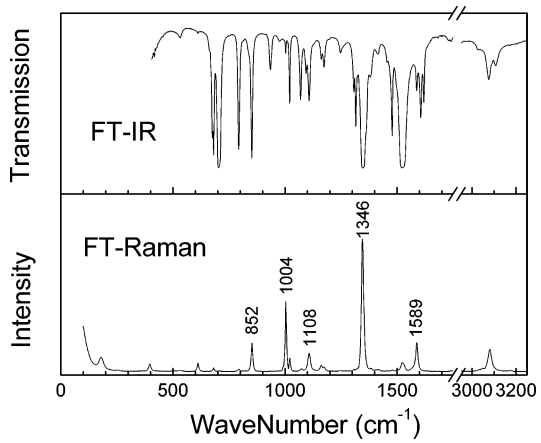

Figure 2. FT-IR (top) and FT-Raman (bottom) spectra of neat nitrobenzene. The wavenumbers (in reciprocal centimeters) of the infrared bands and Raman shifts for the fundamental bands of interest are indicated above the vibrational bands (also see Table 2 for tentative vibrational assignments).

Figure 4 presents an expanded view of the resonance Raman spectrum obtained with 252.7 nm excitation with tentative vibrational assignments indicated above the spectrum. The spectra shown in Figures 3 and 4 have been corrected for sample reabsorption as well as the wavelength dependence response of the detection system. Solvent Raman bands were removed from the spectra by subtracting an appropriately scaled solvent spectrum, and the solvent subtraction artifacts are indicated by asterisks. We note that the intensity of some Raman bands in the spectrum may have contributions from several Raman bands that have very close Raman shifts due to the limited resolution of the solution-phase spectra. Thus, the Raman band labels in Figure 4 only give the largest Raman band contributions to each Raman feature. Most of the resonance Raman features can be assigned to the fundamentals, overtones, and combination bands of about six Franck−Condon active vibrational modes on the basis of the information in Table 2: the nominal NO_2 symmetric stretch ν_{11} (1346 cm^{-1}), the nominal benzene ring stretch ν_7 (1589 cm^{-1}), the nominal ONO symmetry bend/benzene ring stretch ν_{23} (852 cm^{-1}), the nominal C−N stretch/benzene ring breathing ν_{16} (1108 cm^{-1}), the nominal CCC bending ν_{20} (1004 cm^{-1}), and the nominal CCH in-plane bending mode ν_{14} (1174 cm^{-1}).

Time-Dependent Wave Packet Calculations To Model the A-Band 266 and 252.7 nm Resonance Raman Intensities and Absorption Spectrum. We have chosen to model the relative

TABLE 2: Experimental and B3LYP/cc-PVTZ Computed Vibrational Frequencies of Nitrobenzene[a]

		computed		experimental		
sym	modes	B3LYP/cc-PVTZ	b	FT-Raman	FT-IR	descriptions
A_1	ν_1	3227	3130			C−H stretch
	ν_3	3198	3102		3107 w	C−H stretch
	ν_5	3176	3081	3081 m		C−H stretch
	ν_7	1632	1583	1589 m		ring stretch
	ν_9	1517	1471			ring stretch
	ν_{11}	1376	1335	1346 vs		NO_2 symmetric stretch
	ν_{14}	1199	1163	1163 w	1174 m	CCH in-plane bend
	ν_{16}	1120	1086	1108 m	1108 m	C−N stretch + ring breath
	ν_{18}	1046	1015			CCH in-plane bend
	ν_{20}	1025	994	1004 s	1004 mw	CCC trigonal bend
	ν_{23}	869	843	852 m	852 s	ONO symmetric bend + ring stretch
	ν_{27}	698	677	682 w	682 ms	CCC in-plane bend
	ν_{33}	396	384	397 w		ring in-plane bend + C−N stretch
A_2	ν_{21}	1005	975		990	CCH out-of-plane bend
	ν_{24}	862	836		839 w sh	CCH out-of-plane bend
	ν_{32}	421	408			CCC out-of-plane bend
	ν_{36}	52	50			NO_2 torsion
B_1	ν_{19}	1025	994			CCH out-of-plane bend
	ν_{22}	973	944		934 m	CCH out-of-plane bend
	ν_{25}	819	794	794 w	794 s	CCH out-of-plane bend + NO_2 wag
	ν_{26}	725	703		702 vs	CCH out-of-plane bend + NO_2 wag
	ν_{28}	698	677		676 ms	CCH out-of-plane bend
	ν_{31}	449	436			CCC out-of-plane bend
	ν_{35}	170	165	179 w		ring torsion
B_2	ν_2	3227	3130		3107 w	C-H stretch
	ν_4	3189	3093			C-H stretch
	ν_6	1656	1606		1606	ring stretch + NO_2 asymmetric stretch
	ν_8	1592	1544	1524 w		NO_2 asymmetric stretch + ring stretch
	ν_{10}	1494	1449			ring stretch
	ν_{12}	1353	1312			ring stretch
	ν_{13}	1344	1304			CCH in-plane bend
	ν_{15}	1187	1151		1162 s	CCH in-plane bend
	ν_{17}	1102	1069		1069 s	CCH in-plane bend
	ν_{29}	628	609	611 w		CCC in-plane bend
	ν_{30}	526	510			NO_2 asymmetric bend + CCH in-plane bend
	ν_{34}	257	249	256 vw		CCH in-plane bend

[a] Qualitative intensity descriptions: vs = very strong, s = strong, m = medium, w = weak, vw = very weak, sh = shoulder of larger band. [b] These values are scaled by a factor of 0.97.

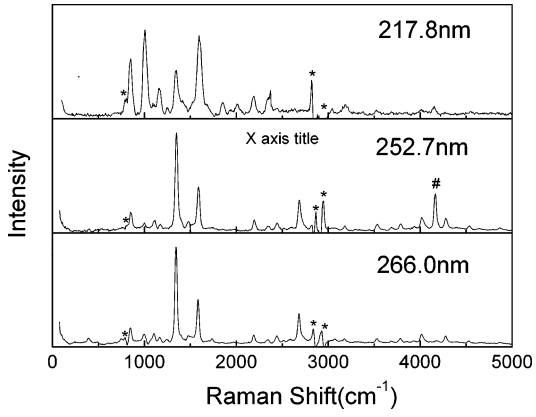

Figure 3. Overall view of the A-band resonance Raman spectra of nitrobenzene in cyclohexane solvent obtained with the excitation wavelengths (in nanometers) indicated next to each spectrum. The spectra have been intensity-corrected and solvent-subtracted. (*) Regions where solvent subtraction artifacts are present; (#) laser line artifact.

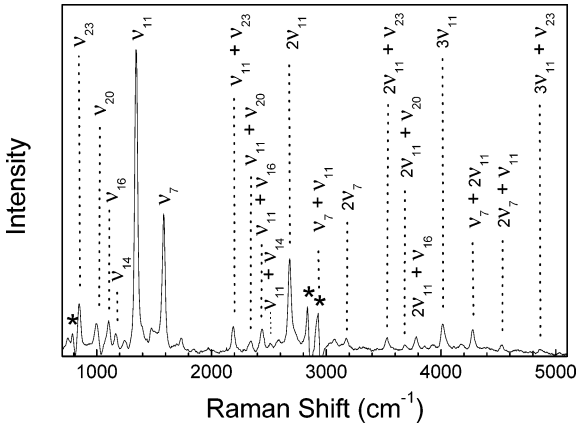

Figure 4. Expanded view of the 266 nm resonance Raman spectrum of nitrobenzene in cyclohexane solvent. The spectrum has been intensity-corrected and solvent-subtracted. Asterisks label parts of the spectrum where solvent subtraction artifacts are present. The tentative assignments to the larger Raman band features are also shown.

intensities of the 266 and 252.7 nm resonance Raman spectra since they are clearly mostly on resonance with the CT-band absorption. The 266 and 252.7 nm resonance Raman spectra have progressions of the nominal NO_2 symmetric stretch ν_{11} (1346 cm^{-1}) and its overtones as well as its combination bands with the nominal benzene ring stretch ν_7 (1589 cm^{-1}) and the nominal ONO symmetry bend/benzene ring stretch ν_{23} (852 cm^{-1}). The absorption spectra and absolute resonance cross sections were simulated by use of the time-dependent wave packet calculations and simple model described in the Experimental and Computational Methods Section. Table 3 presents the calculated parameters that best fit the data for nitrobenzene in the liquid absorption spectra and the intensities of the resonance Raman spectra. To simultaneously fit the absorption bandwidth and the pattern of the resonance Raman intensities, we needed to include a large amount of electronic dephasing

TABLE 3: Parameters for Time-Dependent Wavepacket Calculations and the Resulting Vibrational Reorganization Energy for Nitrobenzene[a]

vibrational mode	frequencies (cm^{-1})	$\|\Delta\|$	vibrational reorganization energy λ_v (cm^{-1})
ν_{23}	849	0.9	344
ν_{20}	1002	0.64	205
ν_{16}	1117	0.66	243
ν_{14}	1174	0.22	28
ν_{11}	1350	1.68	1905
ν_7	1589	0.9	644
			total = 3369

[a] Transition length $M = 0.955$, $E_{00} = 36\,800\ cm^{-1}$, $\Gamma = 580\ cm^{-1}$, G (standard deviation) $= 500\ cm^{-1}$.

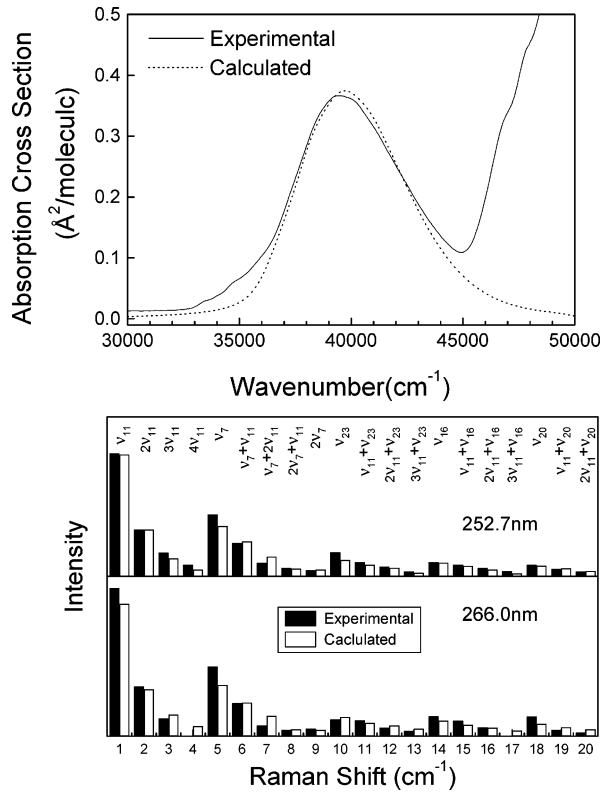

Figure 5. (Top) Comparison of the computed absorption spectrum (···) with the experimental absorption spectrum (—). (Bottom) Comparison of the computed resonance Raman cross sections (open bars) with the experimental Raman cross sections (solid bars) for the main Raman features of the 266 and 252.7 nm resonance Raman spectra. The computations made use of the model described in refs 16−19 with the simple exponential decay dephasing treatment for the solvent (see text for details).

(the Γ parameter) and a large amount of inhomogeneous broadening (the G parameter) in the calculations. This is similar to our previous work on gas- and solution-phase B-band nitroalkanes,[18,19] where large damping parameters were needed to simultaneously fit the absolute Raman cross sections, the relative Raman intensity patterns, and the absorption band. This indicates that the population decay/electronic dephasing occurs substantially faster than just wave packet motion away from the Franck−Condon region.

Since the CT-band resonance Raman spectra of nitrobenzene could possibly be susceptible to interference from preresonance−resonance effects[16,34,47] from higher energy states, we have given greater weight to fitting the larger overtones and combination band features. The top panel of Figure 5 shows a comparison of the calculated absorption spectrum (···) with the experimental (—) absorption spectrum. Figure 5 (bottom panel) and Table S-1 of the Supporting Information also show comparisons of the calculated resonance Raman cross sections (open bars) with the experimental Raman cross sections (solid bars) for the 20 main Raman features of the 266 and 252.7 nm resonance Raman spectra.

Inspection of Figure 5 shows that there is reasonable agreement between the calculated and experimental absorption spectra. The calculated spectrum is consistent with the oscillator strength of the CT transition while simultaneously providing a good fit to the absolute Raman intensities of the 266 and 252.7 nm spectra as shown in lower part of Figure 5. If any of the parameters in Table 3 are changed beyond their estimated uncertainties (about ±5−10%), the calculated fit to the absorption spectrum and/or resonance Raman cross section becomes noticeably poorer. The overall best fit to both the absorption spectrum and the absolute resonance Raman intensities is reasonable to extract the major features of the transition and its associated short-time dynamics on the excited-state potential energy surface.

Examination of the $|\Delta|$ dimensionless parameters determined by fitting the absorption spectrum and the resonance Raman cross sections shows that the largest changes in the displacements occur with the nominal NO_2 symmetry stretch mode ν_{11} ($|\Delta| = 1.68$) and the nominal benzene ring symmetric stretch mode ν_7 ($|\Delta| = 0.9$). There are also more modest contributions from the nominal C−N stretch/benzene ring symmetric breath mode ν_{16} ($|\Delta| = 0.66$), the nominal CCC bend mode ν_{20} ($|\Delta| = 0.64$), the nominal ONO symmetry bend/benzene ring stretch ν_{23} ($|\Delta| = 0.9$), and the nominal CCH in-plane bending mode ν_{14} ($|\Delta| = 0.22$). Our results indicate that the short-time photodissociation dynamics of nitrobenzene have significant multidimensional character, predominantly in the nominal NO_2 symmetric stretch and the nominal benzene ring symmetric stretch mode, accompanied by moderate contributions from the nominal C−N stretch, the nominal CCC bend, and the nominal ONO symmetry bend modes.

Comparison of the Franck−Condon Region Dynamics of Nitrobenzene to Those of *p*-Nitroaniline and Nitroalkanes. *p*-Nitroaniline (PNA) is more strongly charge-transferring in nature than nitrobenzene and is a prototypical charge-transfer molecule for which resonance Raman intensity analysis was carried out.[55] While the absorption spectrum of PNA in cyclohexane solution is shifted about 9000 cm^{-1} to the red of nitrobenzene, the resonance Raman intensity patterns of PNA are basically quite similar to those of nitrobenzene. This is especially true for the three largest Δ modes: the symmetric NO_2 stretch at 1338 cm^{-1} ($\Delta = 1.43$), the benzene ring stretch at 1599 cm^{-1} ($\Delta = 0.496$), and the NO_2 scissors at 859 cm^{-1} ($\Delta = 0.88$) for PNA in cyclohexane are quite close to the symmetric NO_2 stretch at 1350 cm^{-1} ($\Delta = 1.65$), the benzene ring stretch at 1589 cm^{-1} ($\Delta = 0.9$), and the NO_2 scissors at 849 cm^{-1} ($\Delta = 0.9$) for nitrobenzene in cyclohexane. This might indicate that while the substitution of a *p*-H atom of benzene ring by an amino group lowers considerably the electronic transition energy for the phenyl highest occupied molecular orbital (HOMO) to the nitro lowest unoccupied molecular orbital (LUMO), it does not substantially alter the initial nature of the Franck−Condon region photodissociation dynamics.

It is very interesting to compare the CT-band resonance Raman spectra and short-time photodissociation dynamics of nitrobenzene with those of the B-band resonance Raman spectra and short-time photodissociation dynamics of several nitroalkanes.[18,19] First, the B-band absorption spectra for the nitroal-

kanes are broad and structureless at about 200 nm due to a $\pi \rightarrow \pi^*$ transition localized on the NO_2 chromophore. The B-band resonance Raman spectra of the nitroalkanes are all very similar to one another, with most of the Raman intensity appearing in the symmetric NO_2 stretch progression of peaks ($n\nu_{NO_2}$). The modeling of the B-band absorption and resonance Raman intensities of nitroalkanes suggests that electronic dephasing due to population decay (predissociation) and/or solvent collisions takes place substantially faster than the wave packet motion out of the Franck−Condon region. The lack of significant substituent effects on the B-band Franck−Condon region photodissociation dynamics and corresponding resonance Raman spectra of nitroalkanes is probably due to a clear separation of the time scale for motion on the initial excited-state potential energy surface compared with vibrational motion in the rest of the molecule. This would help explain why the intensity pattern of the predominant NO_2 symmetric stretch overtone progression tends to be preserved even as the nitroalkanes become heavier and more branched. In contrast, the CT-band resonance Raman spectra of nitrobenzene display significantly different Raman intensity patterns from those of the nitroalkanes previously studied. The multidimensionality of the Franck−Condon region CT-band photodissociation dynamics of benzene and its obvious substitutent effects suggest that the time scale for the wave packet motion on the initial excited-state potential energy surface is comparable to the vibrational motion in the rest of the molecule. This is most likely due to the delocalized π(benzene ring) $\rightarrow \pi^*(NO_2)$ transition, which is characteristically an intramolecular charge-transfer excitation or a very strong excited-state electronic coupling between the nitro and benzene group in the nitrobenzene molecule. This distinct difference in the nature of the electronic transitions in nitrobenzene and nitroalkanes leads to noticeable differences in the short-time photodissociation dynamics of these types of nitro compounds. Comparison of the normal mode displacements and the vibrational reorganizational energies found from the CT-band resonance Raman spectra of nitrobenzene to those previously found for nitromethane reveals some interesting differences. Table 3 shows that the total vibrational organizational energy associated with the CT-band transition of nitrobenzene is relatively small (about 3369 cm^{-1}) compared to those associated with the B-band transition of nitroalkanes (about 4700 cm^{-1} for the nitromethane, about 6180 cm^{-1} for the nitroethane, and 6255 cm^{-1} for the nitropropane).[18,19] We note from Table 3 that, among the 3369 cm^{-1} total vibrational organizational energy of nitrobenzene, only 1905 cm^{-1} is partitioned into the NO_2 symmetry stretch mode, while among the 4700 cm^{-1} total vibrational organizational energy determined from the B-band resonance Raman intensity analysis of nitromethane (or the 6180 cm^{-1} for the nitroethane and the 6255 cm^{-1} for the nitropropane), almost all of the energy is allocated to the NO_2 symmetry stretch mode. A simple qualitative explanation for this result is the following: electronic excitation in the nitroalkanes involves taking an electron from a π-bonding orbital on the nitro group and placing it into a π-antibonding orbital on that group, whereas in nitrobenzene an electron is taken from a nominally π-bonding orbital on the phenyl group and placed into a π-antibonding orbital of nitro group. The net change in the π-bond order for the nitro group should be greater in the former case than in the latter case. Further support for this explanation comes from a molecule containing a $=C(-C\equiv N)_2$ group where the vibrational reorganization energy for the locally excited transition of the $=C(-C\equiv N)_2$ group is larger than that for the charge-transfer transition of that group.[56]

The dissociation of nitroalkanes was predicted through both the excited-state C−N bond rupture channel (major) and the isomerization (to methyl nitrite, CH_3ONO, and subsequent dissociation to CH_3O and NO) channel (minor).[15] However, the dissociation pathways of nitrobenzene were predicted to occur mainly through the isomerization channel (to phenyl nitrite, C_6H_5ONO, and then subsequent dissociation to C_6H_5O and NO). The significant difference in the vibrational reorganizational energy of NO_2 symmetry stretch mode distributions could be one of the important factors that influences the partitioning into the exit channels.[24] Li et al.[24] performed B3LYP/6-31G* calculations, found the energy barrier for isomerization of nitrobenzene to phenylnitrite by locating its transition state, and determined the barrier to be 63 kcal/mol. We carried out similar B3LYP/6-31G* calculations for nitromethane and nitroethane and obtained energy barriers of 72 kcal/mol for the isomerization of nitromethane to methylnitrite and 69 kcal/mol for the isomerization of nitroethane to ethylenitrite. The energy barrier for the isomerization of nitrobenzene to phenylnitrite is lower by about 6−9 kcal/mol than those for the nitroalkanes. Energetically, 200 nm excitation for nitroalkanes results in a total energy of 143 kcal/mol, while 252.7 nm excitation for nitrobenzene results in a total energy of 113 kcal/mol. The energy difference between the transition state of the ground-state isomerization and the B-band initial state of nitromethane for 200 nm excitation is 71 kcal/mol. For nitrobenzene with 252.7 nm excitation, the value is only 50 kcal/mol, which is significantly lower than that for nitromethane by about 20 kcal/mol on the basis of the B3LYP-TD/6-31G* computations. This could suggest that the lower energy difference between the ground-state isomerization and the excited-state dissociation potential energy surfaces for nitrobenzene may help favor the isomerization exit channel. On the other hand, the higher energy difference between the ground-state isomerization and the excited-state dissociation potential energy surfaces for nitromethane may help favor the C−N bond rupture exit channel. This possible correlation suggests it may be worthwhile to do further theoretical examination of the relationship between the ground- and excited-state surfaces for nitrobenzene and nitroalkanes to better elucidate how the substituent effects on the potential energy surfaces results in their significantly different photochemical reaction product distributions.

It is also interesting to note that there is a noticeable C−N bond length difference between the transition-state geometries for the isomerization reactions of nitrobenzene and nitromethane. Based on the B3LYP/6-31G* calculations, the C−N bond lengths of the transition-state geometry structures for nitromethane and nitroethane are 1.94 and 2.0 Å, respectively. They are considerably longer than the 1.74−1.78 Å for the analogous isomerization reaction of nitrobenzene to phenylnitrite.[24] This large difference in the C−N bond length for the transition state of the isomerization reactions of nitroalkanes and nitrobenzene might be another important factor that influences the branching ratio of both processes (the isomerization channel and C−N band rupture channel) in these nitro compounds. We note that B-band excitation of nitroalkanes leads to two exit channels: the major $CH_3NO_2 \rightarrow CH_3 + NO_2$ photodissociation channel[11−14] and the minor isomerization channel of nitromethane to methyl nitrite CH_3ONO prior to dissociation.[15] This suggests that there exists a curve crossing between the B-band state and the ground isomerization potential energy surface. Thus, the transition state is thought to be an important point that correlates the B-band excited-state nitroalkanes and the ground-state nitroalkane isomerization product,

alkyl nitrite. The C−N bond length might indicate that the nitroalkane molecule will undergo more geometry reorganization before reaching the transition state. The reorganization energies in Table 3 might suggest that there could be a correlation between the C−N bond length of the transition structure and the reorganization energies.

We note that our resonance Raman spectra of nitrobenzene in cyclohexane solution in the CT band absorption are dominated by six totally symmetric modes. The photodissociation of nitrobenzene is predicted by ab initio computations to occur via an initial isomerization to phenyl nitrite. If this occurs at a very early stage or in the Franck−Condon region, then asymmetric bending and/or stretching of the NO_2 group should occur. Our results suggests that the isomerization processes do not take place at very early times and instead take place somewhere after the wave packet leaves the Franck−Condon region.

Conclusions

CT-band resonance Raman spectra were acquired for nitrobenzene in cyclohexane solution and a preliminary resonance Raman intensity analysis was done. The resonance Raman spectra and intensity analysis indicate that most of the short-time photodissociation dynamics in the Franck−Condon region occurs along the nominal NO_2 stretch and nominal benzene ring symmetry stretch normal modes, accompanied by smaller components along the nominal ONO symmetry bend/benzene ring stretch mode, the nominal C−N stretch/benzene ring breathing mode, the nominal CCC bending mode, and the nominal CCH in-plane bending mode. These results for nitrobenzene were compared to those previously reported for several nitroalkanes. The short-time dynamics for nitrobenzene were found to be noticeably different from those of nitroalkanes with substantially less vibrational reorganizational energy taking place in the Franck−Condon region of nitrobenzene compared to the nitroalkanes. We briefly discussed possible implications for this behavior and results for preliminary reaction pathway calculations.

Acknowledgment. This work was supported by grants from NSFC (Grant 20273062), EYTP, MOE of China (Grant 1918), and ZJNSF (Grant 201019) of China to X.Z. and from the Research Grants Council (RGC) of Hong Kong (HKU 7021/03P) to D.L.P.

Supporting Information Available: Table S-1, showing a comparison of the calculated and experimental resonance Raman cross sections for the 252.7 and 266 nm resonance Raman spectra of nitrobenzene, and Cartesian coordinates, total energies, and vibrational zero-point energies for selected stationary structures for the isomerization reactions of nitrobenzene, nitromethane, and nitroethane as described in the text (doc, PDF). This material is available free of charge via the Internet at http://pubs.acs.org.

References and Notes

(1) Kondridov, B. N.; Kozad, G. D.; Raikova, V. M.; Starshinov, A. V. *Sov. Phys. Dokl. Phys. Chem.* **1977**, *233*, 402−405.

(2) Tsang, W.; Robaugh, D.; Mallard, W. *J. Phys. Chem.* **1986**, *90*, 5968−5973.

(3) Kwok, H. S.; He, G. Z.; Sparks, R. K.; Lee, Y. T. *Int. J. Chem. Phys.* **1981**, *13*, 1125−1131.

(4) Turnipseed, A. A.; Vaghjiani, G. L.; Thompson, J. E.; Ravishankara, A. R. *J. Chem. Phys.* **1992**, *96*, 5887−5895.

(5) Nagakura, S. *Mol. Phys.* **1960**, *3*, 152−162.

(6) Harris, L. E. *J. Chem. Phys.* **1973**, *58*, 5615−5626

(7) Flicker, W. M.; Mosher, O. A.; Kuppermann, A. *Chem. Phys. Lett.* **1979**, *60*, 518−522.

(8) Flicker, W. M.; Mosher, O. A.; Kuppermann, A. *J. Chem. Phys.* **1980**, *72*, 2788−2794.

(9) Kleier, D. A.; Lipton, M. A. *J. Mol. Struct.: THEOCHEM* **1984**, *109*, 39−49.

(10) Mijoule, C.; Odiot, S.; Fliszar, S.; Schnur, J. M. *J. Mol. Struct.: THEOCHEM* **1987**, *149*, 311−321.

(11) Butler, L. J.; Drajnovich, D.; Lee, Y. T.; Ondrey, G.; Bersohn, R. *J. Chem. Phys.* **1983**, *79*, 1708−1722.

(12) Blais, N. C. *J. Chem. Phys.* **1983**, *79*, 1723−1731.

(13) Lao, K. Q.; Jensen, E.; Kash, P. W.; Butler, L. J. *J. Chem. Phys.* **1990**, *93*, 3958−3969.

(14) Moss, D. B.; Trentelman, K. A.; Houston, P. L. *J. Chem. Phys.* **1992**, *96*, 237−247.

(15) Wodtke, A. M.; Hintsa, E. J.; Lee, Y. T. *J. Phys. Chem.* **1986**, *90*, 3549−3558.

(16) Phillips, D. L.; Myers, A. B. *J. Phys. Chem.* **1991**, *95*, 7164−7171.

(17) Lee, C. W.; Zheng, X.; Phillips, D. L. *Asian J. Spectrosc.* **1999**, *3*, 69−77.

(18) Kwok, W. M.; Hung, M. S.; Phillips, D. L. *Mol. Phys.* **1996**, *88*, 517−531.

(19) Hung, M. S.; Kwok, W. M.; Phillips, D. L. *Mol. Phys.* **1998**, *93*, 173−180

(20) Robin, M. R. *Higher excited states of polyatomic molecules*; Academic Press: New York, 1975; Vol. II, p 251.

(21) Kröhl, O.; Malsch, K.; Swiderek, P. *Phys. Chem. Chem. Phys.* **2000**, *2*, 947−953

(22) Galloway, D. B.; Bartz, J. A.; Huey, L. G.; Crim, F. F. *J. Chem. Phys.* **1993**, *98*, 2107−2114.

(23) Clenewinkel-Meyer, T.; Crim, F. F. *J. Mol. Struct.: THEOCHEM* **1995**, *337*, 209−224.

(24) Li, Y. M.; Sun, J. L.; Yin, H. M.; Han, K. L.; He, G. Z. *J. Chem. Phys.* **2003**, *118*, 6244−6249.

(25) Castle, K. J.; Abbott, J.; Peng, X. Z.; Kong, W. *J. Chem. Phys.* **2000**, *113*, 1415−1419.

(26) Kosmidis, C.; Ledingham, K. W. D.; Kilic, H. S.; McCanny, T.; Singhal, R. P.; Langley, A. J.; Shaikh, W. *J. Phys. Chem. A* **1997**, *101*, 2264−2270.

(27) Shao, J.; Baer, T. *Int. J. Mass Spectrom. Ion. Processes* **1988**, *86*, 357−367.

(28) Marshall, A.; Clark, A.; Ledingham, K. W. D.; Sander, J.; Singhal, R. P. *Int. J. Mass Spectrom. Ion. Processes* **1993**, *125*, R21−R26.

(29) Asher, S. A. *Annu. Rev. Phys. Chem.* **1988**, *39*, 537−588.

(30) Kwok, W. M.; Phillips, D. L. *Chem. Phys. Lett.* **1995**, *235*, 260−267.

(31) Phillips, D. L.; Kwok, W. M. *Chem. Phys. Lett.* **1995**, *241*, 267−274.

(32) Man, S. Q.; Kwok, W. M.; Phillips, D. L. *J. Phys. Chem.* **1995**, *99*, 15705−15708.

(33) Kwok, W. M.; Phillips, D. L. *J. Chem. Phys.* **1996**, *104*, 2529−2540.

(34) Kwok, W. M.; Phillips, D. L. *J. Chem. Phys.* **1996**, *104*, 9816−9832.

(35) Man, S.-Q.; Kwok, W. M.; Johnson, A. E.; Phillips, D. L. *J. Chem. Phys.* **1996**, *105*, 5842−5857.

(36) Kwok, W. M.; Ng, P. K.; He, G. Z.; Phillips, D. L. *Mol. Phys.* **1997**, *90*, 127−139.

(37) Phillips, D. L.; Myers, A. B. *J. Raman Spectrosc.* **1997**, *28*, 839−848.

(38) Zheng, X.; Phillips, D. L. *Chem. Phys. Lett.* **1998**, *286*, 79−87.

(39) Zheng, X.; Phillips, D. L. *Chem. Phys. Lett.* **1998**, *292*, 295−306.

(40) Zheng, X.; Phillips, D. L. *J. Chem. Phys.* **1998**, *108*, 5772−5783.

(41) Zheng, X.; Phillips, D. L. *Chem. Phys. Lett.* **1999**, *307*, 350−358.

(42) Zheng, X.; Phillips, D. L. *Chem. Phys. Lett.* **1998**, *296*, 173−182.

(43) Zheng, X.; Lee, C. W.; Phillips, D. L. *J. Chem. Phys.* **1999**, *111*, 11034−11043.

(44) Lee, S. Y.; Heller, E. J. *J. Chem. Phys.* **1979**, *71*, 4777−4788.

(45) Heller, E. J.; Sundberg, R. L.; Tannor, D. J. *J. Phys. Chem.* **1982**, *86*, 1822−1833.

(46) Myers, A. B.; Mathies, R. A. In *Biological Applications of Raman Spectroscopy*; Spiro, T. G., Ed.; Wiley: New York, 1987; Vol. 2, p 1.

(47) Myers, A. B. In *Laser Techniques in Chemistry*; Myers, A. B., Rizzo, T. R., Eds.; Wiley: New York, 1995; p 325.

(48) Becke, A. *J. Chem. Phys.* **1986**, *84*, 4524−4529.

(49) Lee, C.; Yang, W.; Parr, R. G. *Phys. Rev. B* **1988**, *37*, 785−789.

(50) Frisch, M. J.; Trucks, G. W.; Schlegel, H. B.; Scuseria, G. E.; Robb, M. A.; Cheeseman, J. R.; Zakrzewski, V. G.; Montgomery, J. A., Jr.; Stratmann, R. E.; Burant, J. C.; Dapprich, S.; Millam, J. M.; Daniels, A. D.; Kudin, K. N.; Strain, M. C.; Farkas, O.; Tomasi, J.; Barone, V.; Cossi, M.; Cammi, R.; Mennucci, B.; Pomelli, C.; Adamo, C.; Clifford, S.; Ochterski, J.; Petersson, G. A.; Ayala, P. Y.; Cui, Q.; Morokuma, K.; Malick, D. K.; Rabuck, A. D.; Raghavachari, K.; Foresman, J. B.; Cioslowski, J.;

Ortiz, J. V.; Baboul, A. G.; Stefanov, B. B.; Liu, G.; Liashenko, A.; Piskorz, P.; Komaromi, I.; Gomperts, R.; Martin, R. L.; Fox, D. J.; Keith, T.; Al-Laham, M. A.; Peng, C. Y.; Nanayakkara, A.; Gonzalez, C.; Challacombe, M.; Gill, P. M. W.; Johnson, B.; Chen, W.; Wong, M. W.; Andres, J. L.; Gonzalez, C.; Head-Gordon, M.; Replogle, E. S.; Pople, J. A. Gaussian 98, revision A.1; Gaussian, Inc.: Pittsburgh, PA, 1998.

(51) Green, J. H. S.; Kynaston, W.; Lindsey, A. S. *Spectrochim. Acta* **1961**, *17*, 486-502.

(52) Stephenson, C. V.; Coburn, W. C.; Wilcox, W. S. *Spectrochim. Acta* **1961**, *17*, 933−946.

(53) Green, J. H. S.; Harrison, D. J. *Spectrochim. Acta. Part A* **1970**, *26*, 1925−1937.

(54) Clarkson, J.; Smith, W. E. *J. Mol. Struct.* **2003**, *655*, 413−422.

(55) Moran, A. M.; Kelley, A. M. *J. Chem. Phys.* **2001**, *115*, 912−925.

(56) Lilichenko, M.; Tittelbach-Helmrich, D.; Verhoeven, J. W.; Gould, I. R.; Myers, A. B. *J. Chem. Phys.* **1998**, *109*, 10958−10969.